Test Environments and Mechanical Properties of Zr-Base Bulk Amorphous Alloys

C.T. LIU, L. HEATHERLY, D.S. EASTON, C.A. CARMICHAEL, J.H. SCHNEIBEL, C.H. CHEN, J.L. WRIGHT, M.H. YOO, J.A. HORTON and A. INOUE

The mechanical properties of two Zr-base bulk amorphous alloys (BAA), Zr-10Al-30Cu-5Ni (BAA-10) and Zr-10Al-5Ti-17.9Cu-14.6Ni (BAA-11), were studied by both tensile and compressive tests at room temperature in various test environments. The BAA ingots up to 7 mm in diameter were successfully produced by both arc melting and drop casting and induction melting and injection casting. The BAA specimens deformed mainly elastically, followed by catastrophic failure along shear bands. Examination of the fracture region revealed ductile fracture features resulting from a substantial increase in temperature, which was attributable to the conversion of the stored elastic strain energy to heat. Surprisingly, ''liquid droplets'' located at major shear-band cracks adjacent to the fracture section were observed, indicating the occurrence of local melting during fracture. The angle orientation of shear bands, shear-band cracks, and fracture surfaces relative to the stress axis is quite different for BAA specimens tested in tension and compression. This suggests that both shear stress and normal stress may play a role in developing shear bands during plastic deformation. The tensile properties of BAAs were found to be insensitive to the test environment at room temperature. However, the reaction of BAAs with distilled water and heavy water was detected by laser desorption mass spectrometry (LDMS). These results suggest that moisture-induced hydrogen embrittlement in BAAs may be masked by catastrophic fracture following shear bands.

I. INTRODUCTION

METALLIC glasses with amorphous structures were first synthesized in 1960.[1] In order to achieve an amorphous state, extremely high cooling rates ($>10^6$ K/s) were required at that time; as a result, only thin-section materials ($<<0.1$ mm) could be produced. Since metallic glasses possess many attractive properties for structural and functional uses, considerable efforts have been devoted for the past 3 decades to the synthesis of metallic glasses with higher glass-forming ability and lower critical cooling rates. The synthesis of metallic glasses in a bulk form (with thickness >1 mm) was successfully achieved in $Ni_{40}Pd_{40}P_{20}$ alloys by Chen[2] in 1976. Substantial progress on the development of new bulk amorphous alloys (BAA) containing no noble-metal elements (such as Pd, Pt) with a high glass-forming ability has been made only in recent years.

Since 1989, the year when BAAs based on La-Al-TM (where TM = transition-metal elements such as Ni, Cu, and Fe) were first discovered,[3] a number of BAAs with critical cooling rates $<10^3$ K/s have been synthesized in multicomponent alloy systems. The stable metallic glass alloy systems bearing no noble-metal elements include La-Al-TM,[3,4] Zr-Al-TM,[5] Zr-Ti-Al-TM,[6] Ti-Zr-TM,[7,8] Ti-Zr-TM-Be,[9,10] and Fe-(Al,Ga)-(P, B, C, Si) compositions.[11,12] Characterization of the atomic arrangement and physical and thermal properties of these BAAs reveals that their high glass-forming ability is related to several metallurgical factors.[8,13–16] First, these BAAs usually contain many elements, ≥3 elements, which results in increased glass-forming ability by increasing the configurational entropy of supercooled liquid phases. Second, the constituent elements have a large difference in atomic size, usually ≥12 pct, thus limiting the solubility of these elements in crystalline states and packing atoms, efficiently resulting in a lowering of the ground-state energy of supercooled liquid phases. Third, BAAs should possess negative heats of mixing, but no single intermetallic phases, such as the Laves and Frank–Casper phases (size compounds), should be stable at these compositions. Fourth, the interstitial and substitutional impurities in BAAs have to be minimized in order to avoid the formation of stable oxides and other compounds. For example, recent studies by Johnson and co-workers[15,17] demonstrate that the cross section of cast Zr-base BAA plates can be increased substantially by reducing the oxygen content in the alloys. The lowering of oxygen content reduces the number of oxygen clusters or oxide particles in molten metals, thereby reducing nuclei for the formation of crystalline phases during cooling.

In spite of the fact that many multicomponent BAAs can be cast into 3- to 16-mm-diameter rods for mechanical-property evaluation, only limited data are available for understanding the mechanical behavior of these BAAs at the

C.T. LIU, Group Leader, L. HEATHERLY and J.A. HORTON, Research Staff Members, D.S. EASTON, Consultant, C.A. CARMICHAEL and J.L. WRIGHT, Technologists, and J.H. SCHNEIBEL and M.H. YOO, Senior Staff Members, are with the Metals and Ceramics Division, Oak Ridge National Laboratory, Oak Ridge, TN 37831-6115. C.H. CHEN, Group Leader, is with the Life Sciences Division, Oak Ridge National Laboratory. A. INOUE, Professor, is with the Institute for Materials Research, Tohoku University, Sendai, 980-8577 Japan.

This article is based on a presentation made at the ''Structure and Properties of Bulk Amorphous Alloys'' Symposium as part of the 1997 Annual Meeting of TMS at Orlando, Florida, February 10–11, 1997, under the auspices of the TMS-EMPMD/SMD Alloy Phases and MDMD Solidification Committees, the ASM-MSD Thermodynamics and Phase Equilibria, and Atomic Transport Committees, and sponsorship by the Lawrence Livermore National Laboratory and the Los Alamos National Laboratory.

present time. One of the reasons is that most advanced BAAs have been developed only within the last 6 years. Bruck *et al.*[18,19] characterized the mechanical properties of $Zr_{41.25}Ti_{13.75}Ni_{10}Cu_{12.5}Be_{22.5}$ BAA by tension, compression, and torsion tests at room temperature. This BAA exhibited an elastic–perfectly plastic deformation behavior, similar to that observed previously in $Pd_{77.5}Cu_6Si_{16.5}$ (Reference 20) and $Pd_{40}Ni_{40}P_{20}$ (Reference 21) amorphous alloys. The BAA showed excellent tensile properties, with a yield strength up to 1.9 GPa and an elastic strain of about 2 pct.[18] By combined tension, compression, and torsion tests, Bruck *et al.* concluded that the Zr-base BAA obeys a pressure-insensitive von Mises yield behavior. The examination of the orientation of the shear bands and failure surfaces, however, does not appear to support the von Mises yield behavior,[20] rather, it tends to support the pressure-sensitive Mohr–Coulomb criterion suggested by Donovan based on studies of the deformation of $Pd_{40}Ni_{40}P_{20}$ amorphous alloys.[21] In order to understand the deformation mechanisms, more studies are required to resolve these conflicting results. The mechanical properties of $Zr_{65}Ni_{10}Cu_{17.5}Al_{7.5}$ were studied also by Bruck.[22] The limited results indicate that the deformation behavior of this BAA is not much different from that of $Zr_{41.25}Ti_{13.75}Ni_{10}Cu_{12.5}Be_{22.5}$. The Be-containing BAA exhibited a veinlike fracture mode,[18] similar to other amorphous alloys.[23,24] The macroscopic stress-strain curves of the Be-containing BAA showed no appreciable plastic deformation in tension; nevertheless, a plastic strain of several percent was observed during compressive tests at room temperature.[18]

Inoue and co-workers[25,26,27] characterized the mechanical properties of Zr-base and Ti-base BAAs by both tensile and compressive tests at room temperature. The BAAs exhibited a fracture strength ranging from 1.4 to 2.0 GPa with tensile elongations up to 2 pct. A small amount of plastic flow accompanied by serrations was detected in tensile tests of $Zr_{60}Al_{10}Co_3Ni_9Cu_{18}$ and $Zr_{55}Al_{10}Ni_{10}Cu_{20}Pd_5$ (Reference 26), although even higher plastic deformation was measured for the BAAs in compression tests. Earlier, Chen[28] reported the observation of serrated plastic flow in Pd- and Pt-based amorphous alloys. The Zr- and Ti-base alloys also showed a vein-pattern type of fracture mode, typical of the fracture of viscous materials.[29] The Young's modulus of the Zr-base BAAs varies from 80 to 100 GPa at room temperature.

At present, all the deformation studies of BAAs have been conducted in air. Recent studies[30,31,32] of intermetallic alloys containing reactive elements such as Al, Si, and Ti indicate that their tensile ductility and fracture behavior are sensitive to test environments at ambient temperatures. The intermetallic alloys exhibit much higher tensile ductility in dry environments than in those containing moisture and hydrogen, such as ambient air. So far, no attempt has been made to characterize the mechanical properties of BAAs in controlled environments. In this article, two Zr-base BAAs were prepared by melting and casting and their mechanical properties were characterized as a function of the test environment at room temperature. Emphasis has been placed on understanding the mechanism governing the macroscopic deformation and fracture in these alloys. A careful examination by scanning electron microscopy (SEM) reveals localized melting at shear-band cracks adjacent to the fracture surface of tensile-fractured specimens.

II. EXPERIMENTAL PROCEDURES

The following two Zr-base alloy compositions were selected for the study of their mechanical properties in various environments at room temperature: Zr-10Al-30Cu-5Ni (BAA-10) (at. pct), developed at Tohoku University (Sendai, Japan)[33] and Zr-10Al-5Ti-17.9Cu-14.6Ni (BAA-11), developed at Caltech (Pasadena, CA).[17] Zone-purified Zr bars (containing 12.3 appm O and 10 appm Hf), together with pure metal elements, were used as charge materials. The alloys were prepared by arc melting in inert gas, followed by (1) drop casting into 7.0-mm-diameter by 7.2-cm-long Cu molds at Oak Ridge National Laboratory (ORNL) (Oak Ridge, TN) (2) injection casting into 5- or 7-mm Cu molds at ORNL, or (3) injection casting into 5-mm Cu molds at Tohoku University. For injection casting, previously arc-melted alloy stock was first induction-melted inside a quartz tube at temperatures >1000 °C in an inert gas chamber and then injected into a Cu mold with a pressure difference of 15 MPa.

Cast alloy bars were sectioned for microstructural analyses. Metallographic specimens were polished on a Syntron and etched in a solution of 40 mL HNO_3 plus 10 drops of HF. Then X-ray diffraction (XRD) and transmission electron microscopy (TEM) were used to characterize the structure of these cast alloys. The XRD was performed on unetched metallographic specimens using Cu K_α radiation. Alloy disks used for TEM were jet-polished in the solution containing 1 part sulfuric acid and 7 parts methanol at −25 °C and then examined by PHILIPS* CM12 microscope.

*PHILIPS is a trademark of Philips Electronic Instruments Corp., Mahwah, NJ.

Drop-cast and injection-cast rods were used to prepare specimens for tensile and compressive tests. Tensile specimens with 2.35- and 3.19-mm gage diameters were fabricated by centerless grinding of 5- and 7-mm-diameter rods, respectively. Tensile tests were conducted at room temperature in various environments, including air, water, dry oxygen (500 torr O_2 pressure), and vacuum (10^{-6} torr). The details of how the test environments were controlled have been reported elsewhere.[30] Tensile tests were initially performed on button-head specimens with a 12.7-mm gage length. Later on, to accurately measure tensile strains, in Instron extensometer with a 12.7-mm gage length was used,

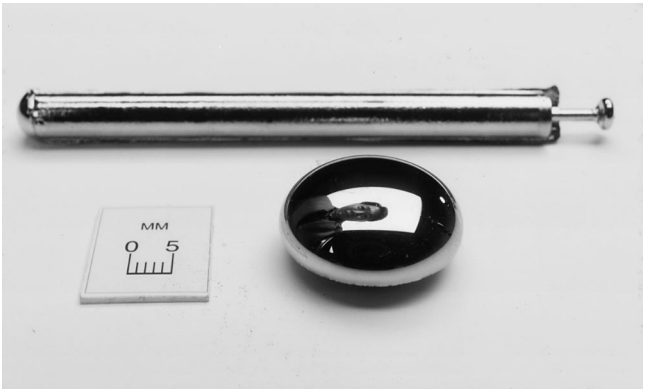

Fig. 1—Zr-based BAA button and ingot prepared by arc melting and drop casting.

and tensile tests were performed on specimens with 17.8-mm gage length. Compression specimens with 17.8-mm diameter were also prepared by grinding, with an aspect ratio of 2:1 (length:diameter). Both tensile and compressive specimens were surface-polished with ''00''-grade SiC papers prior to testing. In order to reduce the frictional stress, the ends of the compressive specimens were lubricated with a lubricating oil. Fracture toughness was determined at room temperature in air by three-point bend testing of edge-notched specimens.[34] The span was 40 mm, the specimen cross section was 5 by 5 mm, and the notch depth was approximately 200 μm. The fracture toughness was calculated from the specimen geometry according to equations given in ASTM standard E-399.

III. RESULTS

Figure 1 shows an arc-melted alloy button and a drop-cast alloy ingot of BAA-11 prepared at ORNL. Free surfaces (such as the top surface of the alloy button) showed a mirror finish. No shrinkage pipes or defects were observed, indicating the absence of large volume changes due to the liquid-to-solid transformation. All these suggest the possible formation of an amorphous structure in the material. The TEM and XRD results are presented in Figure 2. Figure 3 shows that microstructural features were not detected in cast alloy bars. Electron diffraction by TEM shows the formation of an amorphous ring without any diffraction features. The XRD also reveals an amorphous peak without any evidence of crystalline phases in the cast alloy bars. Particles of crystalline phases were observed metallographically in specimens prepared during the early stage of this study, with typical amounts of less than a couple of percent. However, by careful control of the casting environment and the impurities in charge materials, and by superheating the molten liquid prior to drop casting, we could essentially eliminate most crystalline particles. As shown in Figure 3, cast BAA-11 bars contain essentially no crystalline particles and cast cavities.

Tensile tests were performed on both BAA-10 and -11 alloys at room temperature in various test environments, including air, water, vacuum, and dry oxygen. The photo in Figure 4 shows the moment of tensile fracture of a BAA-11 specimen attached to an Instron extensometer. A loud noise, like a firecracker, together with sparking, was detected during the moment of fracture. Table I summarizes the effects of test environment on the room-temperature tensile properties of BAA-10 produced at Tohoku University and ORNL. All the specimens deformed elastically to a level of ~1.5 pct (as measured by the extensometer) followed by catastrophic failure accompanied by a loud noise and sparks. The stress-strain curves show no appreciable macroscopic plastic deformation. The alloy exhibited a high fracture strength, with an average of 1310 MPa for the Tohoku material and 1480 MPa for the ORNL material. It is important to point out that the tensile data (within their scattering band) in Table I show that the test environment has no significant effect on the room-temperature tensile properties of BAA-10.

Table II summarizes the tensile properties of BAA-11 specimens prepared from 7-mm drop-cast alloy bars at ORNL. The tensile data obtained in air and vacuum showed

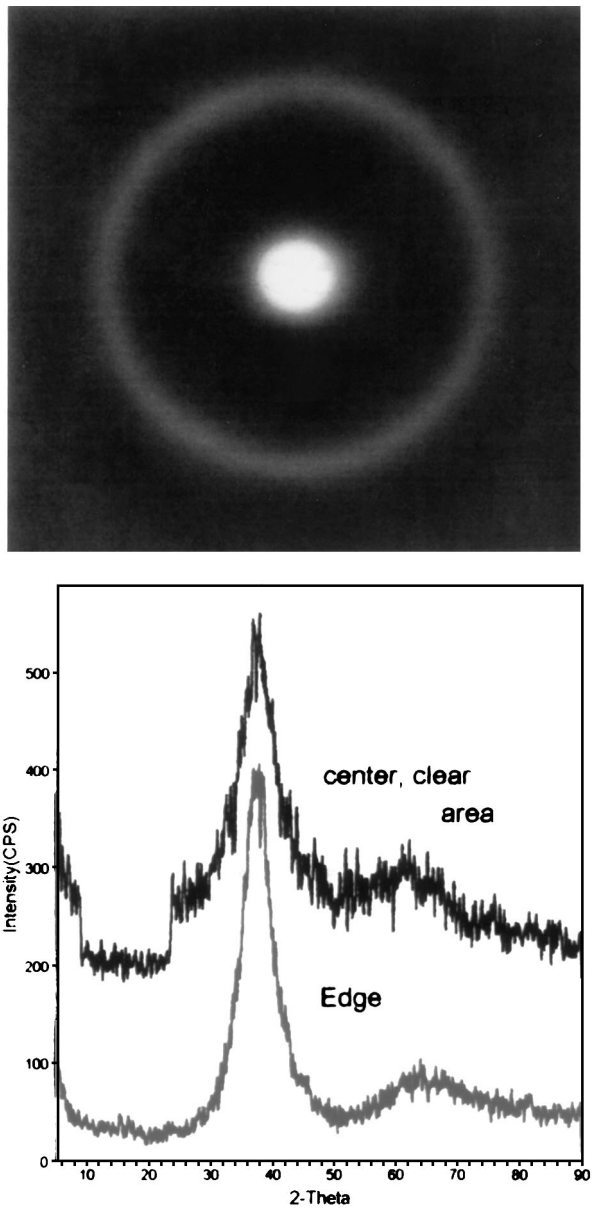

Fig. 2—Electron diffraction and XRD showing the formation of amorphous structures in BAA-11 ingot.

no significant effects of the test environment. The alloy specimens fractured at an average fracture strength of 1680 MPa and an elastic elongation of ~2 pct. Note that BAA-11 exhibited a fracture strength significantly higher (14 pct) than that of BAA-10. From the tensile stress-strain curves, the Young's modulus is determined to be 89 GPa, which agrees well with the moduli of other Zr-base BAAs.[18,25,26]

The compressive properties of BAA-11 are also listed in Table II. As compared with its tensile properties, the alloy showed detectable plastic deformation with an average fracture strength as high as 1870 MPa. Its total strain is around 2.5 pct, with ~0.5 pct plastic strain prior to fracture. Note that the elastic limit obtained from the compressive tests is comparable to the fracture strength from the tensile tests.

The fracture behavior of BAA-10 and -11 was studied by optical micrography as well as SEM. As shown in Figure 5(a), BAA-10 fractured with significant necking at room temperature. Examination of the fracture surface in-

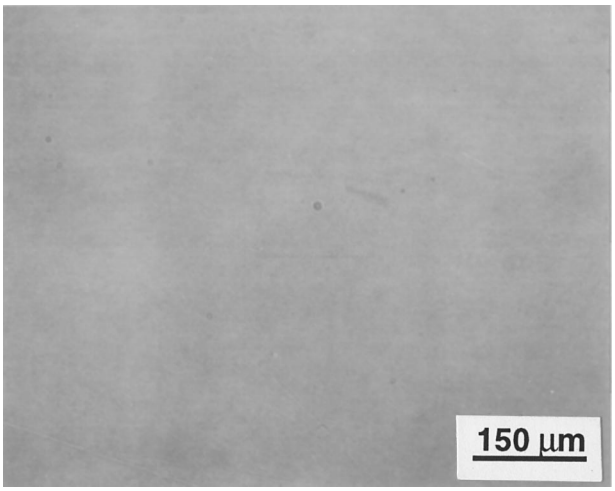

(*a*)

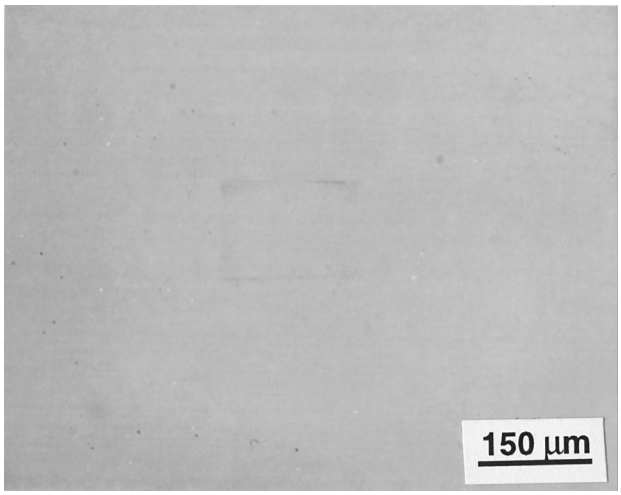

(*b*)

Fig. 3—Optical metallography showing the absence of porosities and crystalline phases in BAA-11 with an amorphous structure: (*a*) not etched and (*b*) etched.

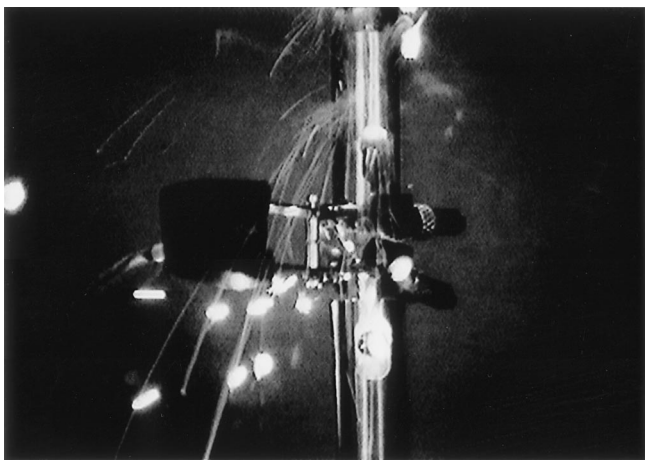

Fig. 4—Photo showing the moment of fracturing a BAA specimen tested at room temperature in air.

dicates that the fracture proceeded mainly by catastrophic shearing. Shear-off steps (~9-μm long) are visible on the outer surfaces near the fracture section (Figure 5(b)). Figure 6 shows macroscopic cracks developing along shear bands, with shear-off steps visible on the specimen outer surfaces.

Figure 7 shows the ductile fracture features for BAA-11 in detail. Here, tensile necking, shear-off lips, macroscopic/microscopic cracks, and cavities are all observed. At higher magnification (Figure 7(b)), metal fibers, presumably formed during the last stage of fracture, are observed, surprisingly, on the central fracture surface. At a tip of the fracture, particles, presumably oxide particles, and voids (formed as a result of the falling out of particles) were found mainly on the outer surfaces (Figure 8). The cause for the formation of these oxide particles and pulled-out fibers will be discussed subsequently.

The fracture mode of selected BAA-10 and -11 specimens was examined by SEM. Vein patterns, commonly associated with the fracture of metallic glasses,[18,19,25–27] fracture steps, and secondary cracks were observed on the fracture surfaces (Figure 9). A cluster of shear-deformation bands close to the fracture section is shown in Figure 10. The average width of these shear bands is around 9 μm. (Note that the fine surface marks with their orientation almost perpendicular to the specimen outer surfaces in Figure 10(a) are grinding marks.) Surprisingly, ''liquid droplets'' located at a major shear-band crack adjacent to the fracture section are clearly visible (Figure 11). Examination of the droplets indicates the possible formation of crystalline phases at their tip.

Table I. Effect of Test Environment on Room-Temperature Tensile Properties of BAA-10 (Zr-10Al-30Cu-5Ni)

Alloy Preparation* (and Ingot Diameter)	Test Environment	Fracture Strength (MPa)	Fracture Strain (Pct)
Alloy Ingots Made at Tohoku University			
IC, 5 mm	water	1210	1.40
IC, 5 mm	air	1310	—
IC, 5 mm	vacuum	1410	—
IC, 5 mm	dry oxygen	1320	—
Alloy Ingots Made at ORNL			
IC, 5 mm	water	1640	1.63
IC, 5 mm	air	1340	1.33
DC, 7 mm	air	1450	1.60

*IC = injection casting. DC = drop casting.

Table II. Effect of Test Environment on Room-Temperature Tensile and Compressive Properties of BAA-11(Zr-10Al-5Ti-17.9Cu-14.6Ni)*

Alloy Number	Test Environment	Elastic Limit (MPa)	Fracture Strength (MPa)	Fracture Strain (Pct)
Tensile Properties				
BAA-11-23	air	—	1650	1.8
BAA-11-16	air	—	1650	2.0
BAA-11-23	vacuum	—	1750	~2.0
BAA-11-28	vacuum	—	1720	~2.0
Compressive Properties				
BAA-11-25	air	1670	1850	2.6
BAA-11-25	air	1770	1880	2.5

*Prepared from drop-cast 7-mm ingots.

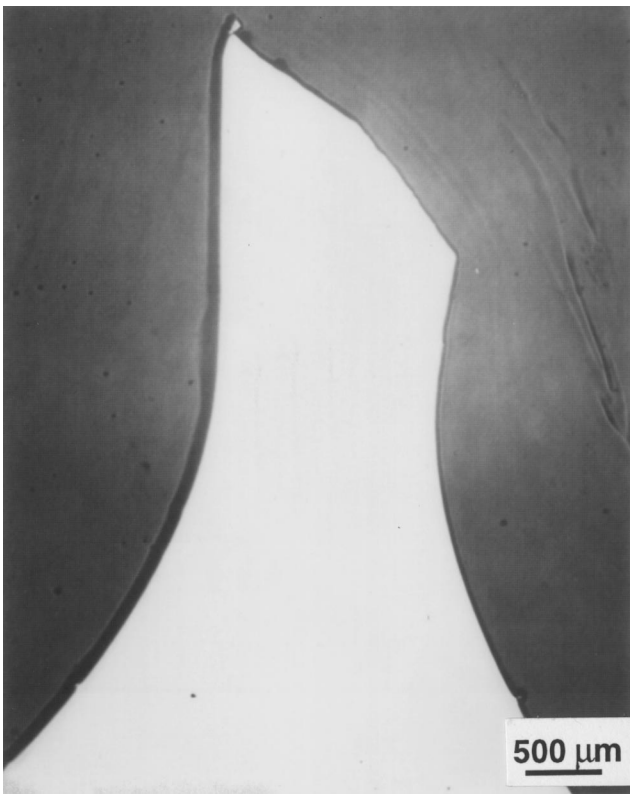

(*a*)

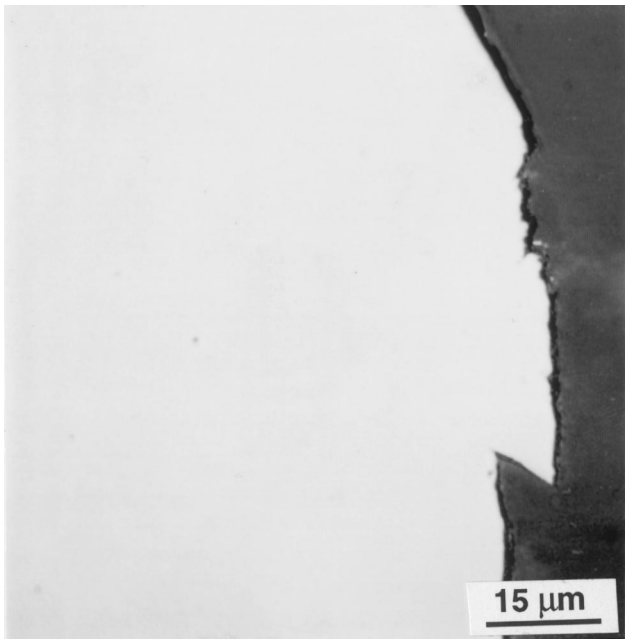

(*b*)

Fig. 5—Optical micrographs showing (*a*) necking and (*b*) shear-off step formed near the fracture section of BAM-10 tensile tested at room temperature.

Table III summarizes the measurement of the orientations of the shear-band steps, shear-band cracks, and fracture surfaces relative to the stress axis. For comparison, the orientation data were obtained for both tensile and compressive specimens. For the compression specimens, the orientation of their fracture surfaces is ~45 deg to the compression axis. For the tensile specimens, the orientation of shear-band steps and cracks and the fracture surfaces varies from $\theta = 53$ to 60 deg relative to the tensile axis for all the specimens examined. The significance of the orientation difference will be discussed subsequently.

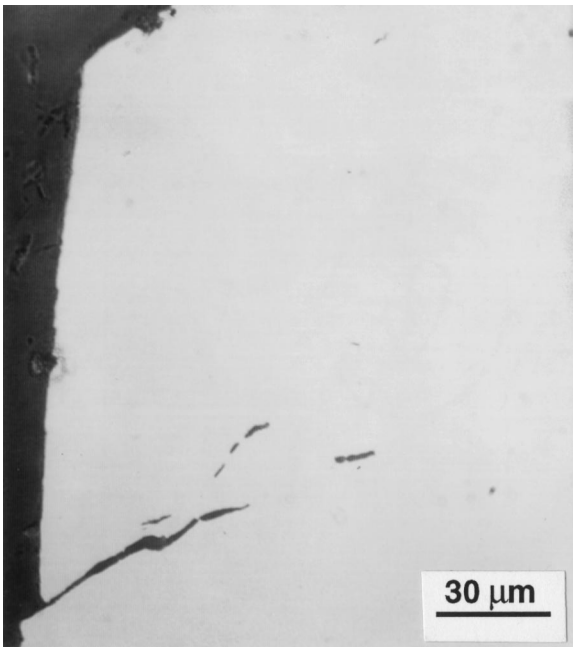

Fig. 6—Optical micrograph showing shear-band cracks formed near the fracture surface of BAM-10 tensile tested at room temperature.

The fracture toughness, K_Q, of BAA-11 was estimated by three-point flexure tests of edge-notched specimens. The results are listed in Table IV. Specimens (1) and (2) exhibited a fracture toughness of 51 to 56 MPa$\sqrt{m}$ at room temperature. A sharp precrack was introduced in specimen (3) by a previous flexure test. The value of K_Q obtained from this specimen in 58 MPa$\sqrt{m}$, not much different from the other two specimens, where the notch crack was produced by cutting.

IV. DISCUSSION

The Zr-base BAAs, particularly BAA-11, exhibited excellent tensile properties at room temperature. The BAA-11 containing 5 at. pct Ti possesses a tensile fracture strength of 1700 MPa with 2 pct elastic strain prior to fracture. The tensile properties of BAA-11 are comparable to those of $Zr_{41.25}Ti_{13.75}Ni_{10}Cu_{125}Be_{225}$ (Reference 18) and $Ti_{40}Zr_{10}Cu_{50}$ (Reference 27). This is the first time that BAAs were tested in different environments, including air, water, vacuum, and dry oxygen at room temperature. The results in Table I and II indicate that the tensile fracture strength and ductility are not sensitive to the test environments. This behavior is quite different from that of intermetallic alloys such as Ni_3Al and FeAl, whose tensile ductility and fracture strength are very sensitive to moisture and hydrogen.

Recent studies[30–32,35] indicate that moisture-induced hydrogen embrittlement is a major cause of brittle fracture and low tensile ductility of ordered intermetallic alloys containing reactive elements such as Al, Si, and Ti tested at ambient temperatures. In the case of aluminides, *e.g.*, FeAl, the embrittlement involves the following chemical reaction:

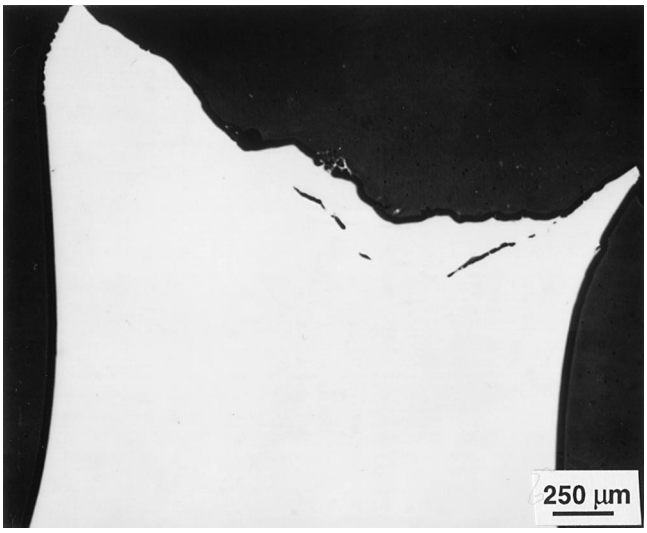

(*a*)

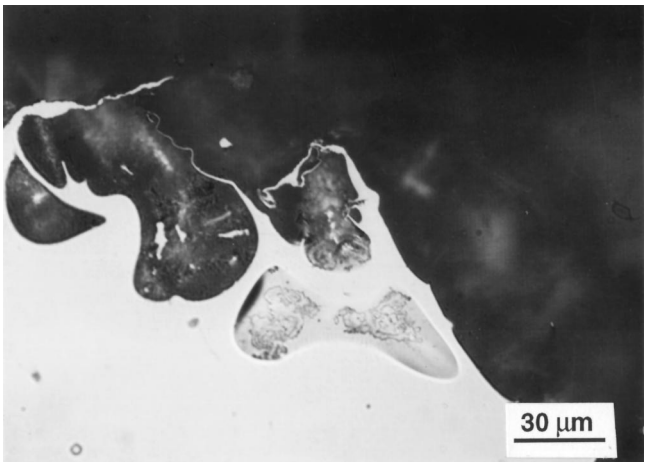

(*b*)

Fig. 7—Optical micrographs showing ductile fracture features observed on the fracture surface of BAA-11 tensile tested at room temperature: (*a*) low magnification and (*b*) high magnification.

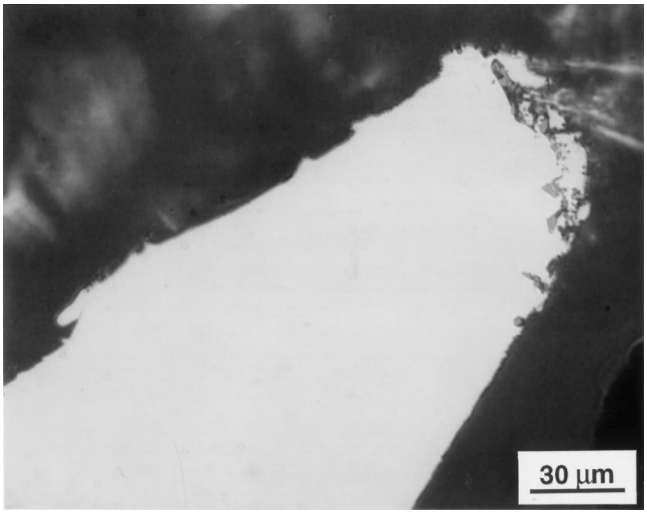

Fig. 8—Optical micrographs showing oxide particles and microcavities observed near the fracture section of BAA-11 tested in tension at room temperature.

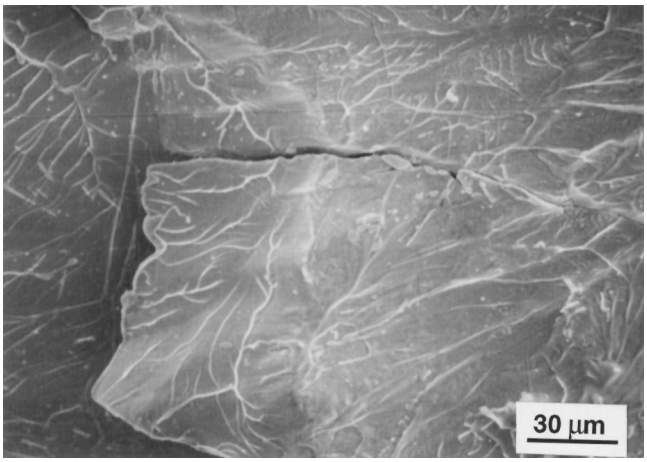

Fig. 9—SEM micrograph showing vein pattern, secondary crack, and fracture step formed on the tensile fracture surface of BAA-11.

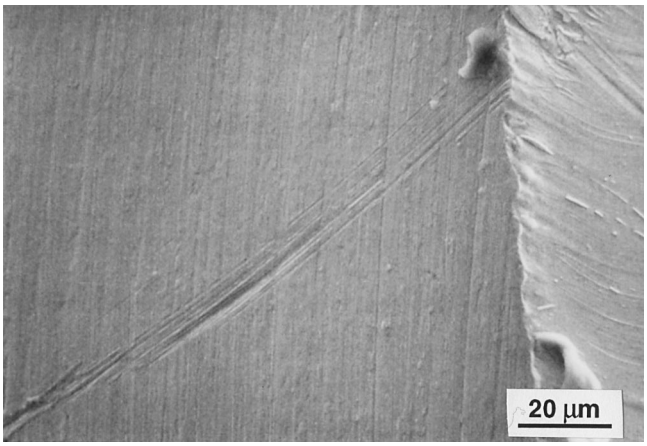

(*a*)

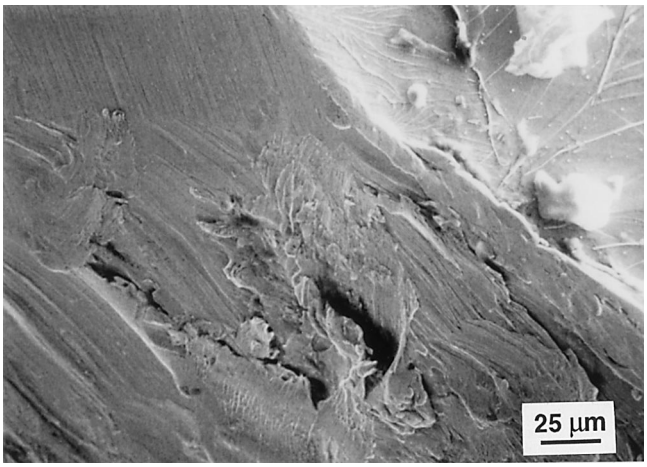

(*b*)

Fig. 10—SEM micrographs showing (*a*) shear-deformation bands and (*b*) ductile cracks formed on the specimen surface near the tensile fracture section of BAA-11.

$$Al + H_2O \rightarrow (AlO) + 2\,(H) \qquad [1]$$

The atomic hydrogen generated from the chemical reaction of Al in FeAl with the moisture in the air penetrates into the alloy and causes severe hydrogen-induced embrittlement during tensile testing at ambient temperatures. This

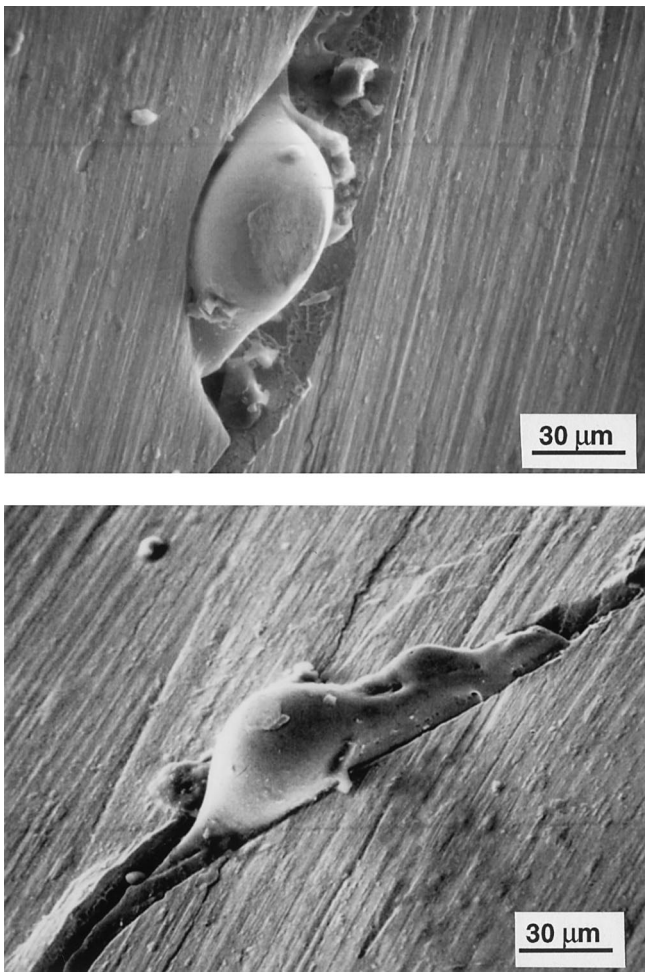

Fig. 11—SEM micrographs showing the formation of liquid droplets, indicating localized melting near the fracture section of BAA-11 tensile fractured at room temperature.

Table III. Comparison of Fracture-Surface and Shear-Band Orientations for BAA Specimens Tested in Tension and Compression at Room Temperature

Test Mode	Alloy Number	Orientation (Relative to the Tensile Axis)		
		Shear-Band Step	Shear-Band Crack	Fracture Surface
Compression	BAA-11	—	—	44 deg*
	BAA-11	—	—	46 deg*
	BAA-11	—	—	44 deg*
Tension	BAA-11	—	—	54 deg**
	BAA-10	60 deg†	—	53 deg**
	BAA-10	56 deg†	56 deg**	58 deg**

*Average values measured from profile projector and visual examination.
**Average values measured from optical micrographs.
†Measured from optical micrographs.

embrittlement can be alleviated by testing FeAl in dry oxygen, which suppresses the formation of atomic hydrogen through the following reaction:

$$2Al + O_2 \rightarrow 2(AlO) \quad [2]$$

and thus causes no embrittlement in FeAl. For instance, an

Table IV. Fracture Toughness (K_Q) of BAA-11 Measured from Three-Point Flexure Tests of Notched Specimens

Specimen Number	Notch Depth, mm	Fracture Load, N	K_Q, MPa$\sqrt{m}$
1	1.89	1037	51
2	1.12	1747	56
3	3.44*	356	58

*Precrack introduced in a previous flexure test.

FeAl alloy, Fe-36.5 pct Al, exhibited a tensile ductility of 17.6 pct in dry oxygen and only 2.2 pct in moist air or in a vacuum backfilled with 67 Pa water vapor.

The BAA-10 and -11 contain large amounts of the reactive elements Zr, Al, and Ti. Based on our understanding of the embrittling mechanism in ordered intermetallic alloys, it is expected that these elements could react with moisture in air or water and generate atomic hydrogen, resulting in moisture-induced hydrogen embrittlement. However, as shown in Table I and II, BAAs showed no such embrittlement. There are two possible reasons for the observation of no moisture-induced hydrogen embrittlement in BAAs:

(1) the moisture in air/water does not react with BAA, thereby generating no hydrogen and causing no embrittlement during tensile testing at room temperature; and
(2) even though hydrogen is generated, the environmental effect is masked by another embrittling mechanism dominating in BAAs.

First, let us check the first possibility. To do so, two BAA-11 samples were used, and both of them were first vacuum-annealed overnight at 100 °C, in order to remove residual hydrogen. One of the samples was then submerged in distilled water (H_2O) and the other one was submerged in heavy water (D_2O), both for 3 days. In order to promote the reaction with water and D_2O, the surfaces of both samples were frequently rubbed against SiC papers in order to create fresh surfaces. The water- and D_2O-treated samples were then quickly placed inside the vacuum chamber of a time-of-flight mass spectrometer at ORNL, and their surfaces were ablated with a high-power laser beam. All elements, including trapped hydrogen and deuterium, were evaporated from sample surfaces, and their mass-to-charge ratio was measured by the time interval between the ablation laser pulse and ion detection in the time-of-flight mass spectrometer.

The results obtained from the laser desorption mass spectrometer (LDMS) are shown in Figure 12. Both H^+ and D^+/H^+ peaks are observed for the D_2O-treated sample. In order to understand these peaks, it is necessary to compare the height of these peaks with those obtained from the H_2O-treated sample. The larger H^+ peak for the H_2O-treated sample indicates that (1) H_2O does react with BAA and generates atomic hydrogen, and (2) the smaller H^+ peak for the D_2O-treated sample was a result of residual hydrogen in BAA even after the vacuum treatment at 100 °C. The distinctly larger D^+/H_2^+ peak for the D_2O-treated sample indicates the reaction of D_2O with BAA and the generation of deuterium in this sample. On the whole, these results provide direct evidence that BAA-11 reacts with moisture and generates atomic hydrogen in this material. A similar

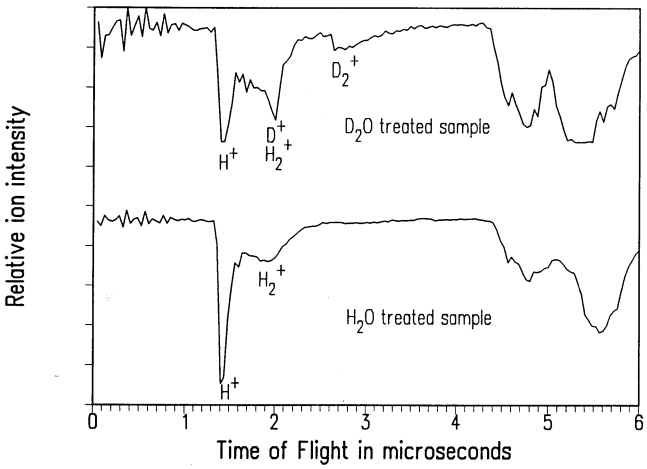

Fig. 12—Comparison of trapped hydrogen and deuterium for BAA-11 samples treated with distilled water and heavy water, respectively. The same laser energy (50 μJ/pulse) was used for both samples.

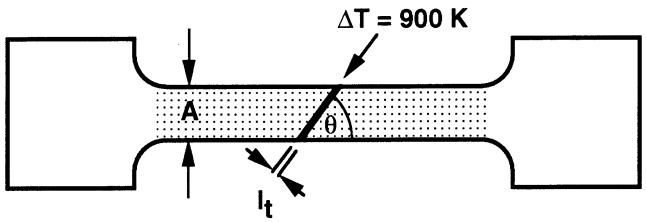

Fig. 13—A sketch showing the concept and parameters used to calculate the local increase in temperature at the moment of tensile fracturing BAA samples.

reaction was observed in FeAl, which showed a substantial reduction of tensile ductility in moist air, caused by moisture-induced hydrogen embrittlement.[30,36] All these results suggest that the moisture-induced hydrogen embrittlement in BAAs may be masked by another embrittling mechanism dominating the brittle fracture and low ductility of BAAs. As evidenced from the study of the fracture morphology, the catastrophic failure of BAAs is essentially caused by the development of localized shear bands at the end of the elastic deformation in BAAs.

The stress-strain curves recorded from the tensile tests of BAAs displayed no appreciable macroscopic plastic deformation prior to catastrophic fracture; however, examination of the fracture region reveals ductile failure at room temperature. As shown in Figures 5 through 10, the features typical of a ductile fracture, including necking, shear lips, voids, microcracks, and tearing marks, are all observed at the fracture of BAAs. The difference in the deformation behavior and in the fracture mode can be rationalized from consideration of localized adiabatic heating occurring at the moment of fracture. The first evidence of a substantial increase in temperature is the observation of metal fibers being pulled out of the fracture surface (Figure 7). The recent study by Inoue[14] showed that bar specimens could be pulled into fine fibers when BAAs were tensile tested at temperatures above T_g (the glass transition temperature). The observation of metal fibers in the BAA specimens tested at room temperature indicates that the local temperature around the fiber region at the moment of fracture reaches above T_g, which is 393 °C for BAA-11. The direct evidence of a local temperature above the melting point is the observation of liquid droplets located at major cracks adjacent to the fracture section (Figure 11). The melting point of BAA-11 is around 850 °C, indicating that the temperature at the shear-band cracks was significantly above 850 °C. It should be pointed out that, by using a high-speed infrared technique, Bruck *et al.*[19] detected an increase in temperature of >500 °C in the shear-band region in $Zr_{41.25}Ti_{13.75}Cu_{12.5}Ni_{10}Be_{22.5}$ when conducting dynamic compressive tests at room temperature.

The local increase in temperature can be estimated from considering the conversion of the stored elastic strain energy to the adiabatic heating of a localized region at the moment of tensile fracture. Figure 13 is a sketch showing the concept and the parameters used in the calculations. The total elastic strain energy (E_e) stored in the gage section prior to fracture is estimated to be 2.45 J, calculated based on the following equation:

$$E_e = (1/2)\ \sigma_f\ \varepsilon_f\ A l_g \qquad [3]$$

where σ_f is the fracture strength, ε_f is the elastic strain at fracture, A is the gage diameter, and l_g is the gage length.

Since all plastic deformation was localized in the shear-deformation bands, it is thus reasonable to assume that all the elastic strain energy is dissipated in the shear-band region at fracture, resulting in the adiabatic heating in that region. The term E_e can thus be correlated with the temperature increase in the shear-band region by the following equation:

$$E_e = C_p\ (\Delta T)\ (A\ \csc\theta) l_t \qquad [4]$$

where C_p is the specific-heat capacity and l_t is the width of the total shear-band region. Since C_p for BAA-11 is not known, C_p = 55 J/K · mole for $Zr_{41.25}Ti_{13.75}Ni_{10}Cu_{12.5}Be_{22.5}$ BAA[9,18,19] is used for calculating l_t in Eq. [4]. By inserting E_e = 2.45 J, ΔT = 900 K, θ = 56 deg, and the molar volume of 12.2×10^{-6} m^3 in Eq. [4], l_t is estimated to be 62 μm. The average width of shear bands is equal to roughly 9 μm (Figure 10). Then, in terms of the number of shear bands heated at fracture, a total of seven shear bands may be heated adiabatically to ΔT = 900 K through the conversion of the elastic strain energy. It appears that the total width of the heated region and the number of shear bands heated at fracture are very reasonable, in view of the fracture morphology observed in BAA-11.

A comparison of the data obtained from tensile and compressive tests sheds light on mechanistic understanding of the deformation and fracture behavior of Zr-base BAAs. As shown in Table II, the elastic limit obtained from the compressive tests is roughly equal to the fracture strength from the tensile tests. This suggests that the fracture occurs upon the development of plastic flow through shear-band formation. There is enough evidence to indicate that the fracture is essentially along shear bands. The BAA-11 showed a plastic strain of ~0.5 pct prior to fracture in compression but not much plastic strain in tension. This suggests the possibility that the fracture in BAAs may be caused not by simply shearing off along shear bands, but rather by a combination of both pulling (related to normal stresses) and shearing (related to shear stresses) at shear bands. Bruck[22] reported that the plastic strain of $Zr_{41.5}Ti_{13.5}Ni_{10}Cu_{12.5}Be_{22.5}$ under compression tests depends on the dimension of cast

ingots, which in turn determines the cooling rate of BAAs. The plastic strain of ~0.5 pct obtained from the compression tests of BAA-11 with a cast ingot size of 7 mm in diameter agrees well with that reported by Bruck.

Shear-band and fracture-surface orientations (relative to the tensile or compressive axis) are different for BAA specimens tested in tension and compression. Since the fracture occurs along the shear bands, the shear-band and fracture-surface orientations are the same, which is $\theta \approx 45$ deg to the compression axis. These compression results suggest that the shear bands are developed along the plane of maximum shear stresses, in agreement with the von Mises yield criterion. In tension, however, the average orientation of shear-band steps, shear-band cracks, and fracture surfaces is $\theta \approx 56$ deg to the tensile axis. As indicated in Figure 14, the increase in θ from 45 to 56 deg results in only a 7 pct decrease in the resolved shear stress, τ, on the shear-band plane, but results in an increase in the tensile normal stress (σ_n) by 37 pct. The observed difference in θ, together with the calculated resolved stresses, suggests that, in addition to the shear stress, the normal stress may play a role in developing shear bands in BAAs. This assertion is reasonable in view of the existence of free volumes and dilations[21,37,38] in BAAs. Further research is certainly required to elucidate the controlling mechanism, in terms of the pressure-insensitive von Mises yield criterion[20] and the pressure-sensitive Mohr–Columb yield criterion,[21] for the deformation and fracture in BAAs.

Table IV shows that BAA-11 has excellent fracture toughness at room temperature. With a fracture toughness above >50 MPa$\sqrt{m}$, there should be no problem with using BAAs as structural engineering materials. For instance, a 7-mm-diameter cast BAA-11 ingot survived an impact test of dropping it on a hard surface from a height of 2 m. The excellent fracture toughness of BAAs may be associated with the high fracture strength together with localized crack-tip plasticity involving shear-band formation. Further studies are required to examine the localized plastic deformation in detail at crack tips.

Oxide particles are observed at the edge of the fracture surfaces in Figure 8. Note that such oxide particles are not observed on other surfaces of tensile-fractured BAA specimens. This suggests the possibility of a substantial increase in temperature, possibly exceeding the melting point, at the fracture tip, resulting in severe surface oxidation. In addition to oxide particles, numerous microcavities are observed at the fracture tip (Figure 8). It is believed that the sparkling observed at the moment of fracture (Figure 4) is attributable to the flying away of ''hot'' oxide particles, leaving microcavities at the oxide sites.

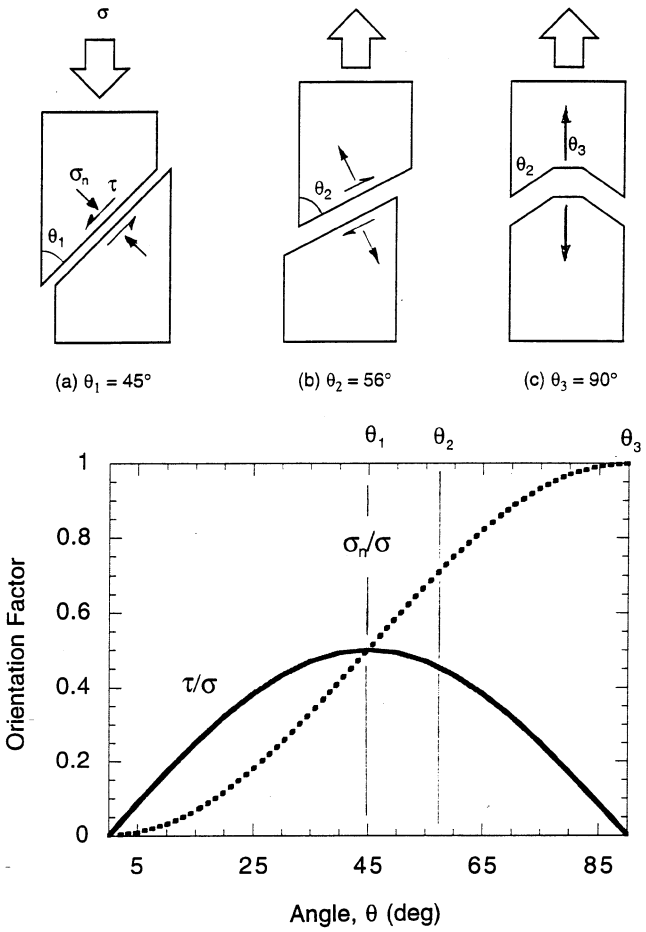

Fig. 14—Effect of resolved shear and normal stresses on shear-band formation and cracking in BAAs.

V. CONCLUSIONS

The mechanical properties of two Zr-base BAAs, BAA-10 and BAA-11, were studied by both tensile and compression tests at room temperature in various test environments, including air, water, vacuum, and dry oxygen. The study has led to the following conclusions.

1. The BAA ingots up to 7 mm in diameter were successfully produced by conventional arc melting and drop casting, and induction melting and injection casting into Cu molds.
2. The Zr-base BAAs, particularly BAA-11, exhibited excellent tensile properties at room temperature. The BAA-11 containing 5 pct Ti possesses a tensile fracture strength of ~1700 MPa with 2 pct elastic strain prior to fracture.
3. The stress-strain curves of the BAAs displayed no appreciable macroscopic plastic deformation prior to catastrophic fracture; however, examination of the fracture region reveals ductile failure at room temperature. This difference in the deformation and fracture behaviors can be rationalized from consideration of localized adiabatic heating, resulting from the conversion of the stored elastic strain energy to heat.
4. A reminiscence of ''liquid droplets'' located at major shear-band cracks adjacent to the fracture surface was observed. A localized surge in temperature exceeding the melting point (= 850 °C for BAA-11) is supported by the thermodynamic calculations based on the conversion of the stored elastic strain energy to the adiabatic heating of the shear-band region.
5. The orientation (θ) of shear bands, shear-band cracks, and fracture surfaces in reference to the stress axis is quite different for BAA specimens tested in tension (θ = 56 deg) and compression (θ = 45 deg). This indicates that both shear stress and normal stress may play a role in developing shear bands during the plastic deformation and fracture.

6. The tensile properties of BAA-10 and -11 are not sensitive to test environment at room temperature. The study by LDMS indicates that the BAAs react with distilled water and heavy water, resulting in the generation of hydrogen and deuterium, respectively. All these results suggest that moisture-induced hydrogen embrittlement in the BAAs may be masked by catastrophic fracture following shear bands.

ACKNOWLEDGMENTS

The authors thank E.D. Specht for X-ray analysis and E.H. Lee for technical assistance. This research was sponsored by the Laboratory Directed Research and Development Program of the Oak Ridge National Laboratory and by the Division of Materials Sciences, United States Department of Energy, under Contract No. DE-AC05-96OR22464, with Lockheed Martin Energy Research Corp. Thanks are also due to E.P. George and L.M. Pike for manuscript review and Connie Dowker for manuscript preparation.

REFERENCES

1. W. Klement, R.H. Wilens, and P. Duwez: *Nature*, 1960, vol. 187, pp. 869-70.
2. H.S. Chen: *Mater. Sci. Eng.*, 1976, vol. 23, pp. 151-54.
3. A. Inoue, T. Zhang, and T. Masumoto: *Mater. Trans., JIM*, 1989, vol. 30, pp. 965-72.
4. A. Inoue, H. Yamaguchi, T. Zhang, and T. Masumoto: *Mater. Trans., JIM*, 1990, vol. 31, pp. 104-09.
5. A. Inoue, T. Zhang, and T. Masumoto: *Mater. Trans., JIM*, 1990, vol. 31, pp. 177-83.
6. A. Inoue, T. Zhang, N. Nishiyama, K. Ohba, and T. Masumoto: *Mater. Trans., JIM*, 1993, vol. 34, pp. 1234-37.
7. A. Inoue, N. Nishiyama, K. Amiya, T. Zhang, and T. Masumoto: *Mater. Lett.*, 1994, vol. 19, pp. 131-35.
8. X.H. Lin and W.L. Johnson: *J. Appl. Phys.*, 1995, vol. 78, p. 6514.
9. A. Peker and W.L. Johnson: *J. Appl. Phys. Lett.*, 1993, vol. 63, pp. 2342-44.
10. W.L. Johnson and A. Peker: in *Science and Technology of Rapid Solidification Processing*, NATO ASI Series E, M. Otooni, ed., 1995, vol. 278.
11. A. Inoue and J.S. Gook: *Mater. Trans., JIM*, 1995, vol. 36, pp. 1180-83.
12. A. Inoue and J.S. Gook: *Mater. Trans., JIM*, 1995, vol. 36, pp. 1282-85.
13. A. Inoue: *Mater. Trans., JIM*, 1995, vol. 36, pp. 866-75.
14. A. Inoue: in *Advanced Materials and Processing*, K.S. Shin, J.K. Yoon, and S.J. Kim, ed., The Korean Institute of Metals and Materials, Seoul, 1995, pp. 1849-58.
15. W.L. Johnson: Caltech, Pasadena, CA 91125, unpublished research, 1997.
16. Akihisa Inoue, Akira Takeuchi, and Tao Zhang: *Metall. Mater. Trans. A*, 1998, vol. 29A, pp. 1779-93.
17. X.L. Lin, W.L. Johnson, and W.K. Rhim: *Mater. Trans., JIM*, 1997, vol. 38, pp. 473-77.
18. H.A. Bruck, T. Christman, A.J. Rosakis, and W.L. Johnson: *Scripta Metall.*, 30, 1994, p. 429.
19. H.A. Bruck, A.J. Rosakis, and W.L. Johnson: *J. Mater. Res.*, 1996, vol. 11, p. 503.
20. H. Kimura and T. Masumoto: in *Amorphous Metallic Alloys*, F.E. Luborsky, ed., Buttersworth and Co., London 1983, p. 187.
21. P. Donovan: *Acta Metall.*, 1989, vol. 37, p. 445.
22. H.A. Bruck: Ph.D. Thesis, California Institute of Technology, Pasadena, CA, 1994.
23. H.J. Leamy, H.S. Chen, and T.T. Wang: *Metall. Trans.*, 1972, vol. 3, pp. 699-708.
24. C.A. Pampillo and A.C. Reimschuesse: *J. Mater. Sci.*, 1974, vol. 9, p. 718.
25. A. Inoue, T. Zhang, and T. Masumoto: *Mater. Trans., JIM*, 1995, vol. 36, pp. 391-98.
26. Y. Yokoyama and A. Inoue: *Mater. Trans., JIM*, 1995, vol. 36, pp. 1398-1402.
27. A. Inoue, K. Amiya, A. Katsuya, and T. Masumoto: *Mater. Trans., JIM*, 1995, vol. 36, pp. 858-65.
28. H.S. Chen: *Rep. Prog. Phys.*, 1980, vol. 43, p. 353.
29. C.A. Pampillo and A.C. Reimschuessel: *J. Mater. Sci.*, 1974, vol. 9, p. 718.
30. C.T. Liu, E.H. Lee, and C.G. McKamey: *Scripta Metall.*, 1989, vol. 23, p. 875.
31. N.S. Stoloff and C.T. Liu: *Intermetallics*, 1994, vol. 2, pp. 75-87.
32. E.P. George, C.T. Liu, and D.P. Pope: *Acta Metall.*, 1996, vol. 44, pp. 1757-63.
33. A. Inoue, T. Zhang, N. Nishiyama, K. Ohba, and T. Masumoto: *Mater. Trans., JIM*, 1993, vol. 34, p. 1234.
34. M.G. Jenkins, A.S. Kobayashi, K.W. White, and R.C. Bradt: *Int. J. Fract.*, 1987, vol. 34, p. 281.
35. K.S. Kumar, C.T. Liu, and J.L. Wright: *Intermetallics*, 1996, vol. 4, pp. 309-18.
36. Y.F. Zhu, C.T. Liu, and C.H. Chen: *Scripta Mater.*, 1996, vol. 35, pp. 1435-39.
37. F. Spaepen: *Acta Metall.*, 1977, vol. 25, p. 407.
38. A.S. Argon: *Acta Metall.*, 1979, vol. 27, p. 47.